Chalmers Publication Library

Active flow control for drag reduction of vehicles using large eddy simulation, experimental investigations and reduced-order modeling

(article starts on next page)

ACTIVE FLOW CONTROL FOR DRAG REDUCTION OF VEHICLES USING LARGE EDDY SIMULATION, EXPERIMENTAL INVESTIGATIONS AND REDUCED ORDER MODELING

Jan Östh[*]**, Siniša Krajnović**[†]

Division of Fluid Dynamics, Department of Applied Mechanics, Chalmers University of Technology,
SE-412 96 Gothenburg, Sweden
E-mail: [*] ojan@chalmers.se, [†] sinisa@chalmers.se

Diogo Barros[1]**, Laurent Cordier**[1]**, Bernd R. Noack**[1]**, Jacques Borée**[1]**, Tony Ruiz**[2]
[1]: Institute PPRIME, CNRS – Université de Poitiers – ENSMA, UPR 3346,
Département Fluides, Thermique, Combustion,
F-86961 Futuroscope Chasseneuil cedex, France, Jacques.Boree@ensma.fr

[2]: Department of Research and Innovation, PSA Peugeot-Citroën
2 route de Gisy, 78943 Vélizy-Villacoublay, France, tony.ruiz@mpsa.com

ABSTRACT

The purpose of this short paper is to introduce first results obtained in a collaborative research between the partners. This research is dedicated to drag reduction of vehicles using LES, experimental investigation and ultimately reduced order modeling. First numerical and experimental results are presented. Experiments show that periodic forcing at high frequencies and amplitudes of the order of the upstream velocities can be viewed as a promising strategy for drag reduction targeted control of three-dimensional bluff-bodies.

1 INTRODUCTION

The development of flow control strategies applied to ground vehicles requires thorough understanding of the flow around them. The major contributor to the aerodynamic drag is associated to the wake region of the body. An active control strategy has the advantage over the passive one as it can adapt to modifications of the flow conditions such as atmospheric turbulence, gusty flow conditions, overtaking, change in speed etc. Although the long term goal of the present work is development of closed-loop flow control, the present paper investigates open-loop flow control around a simplified square-back ground vehicle. Both experimental and numerical techniques (large eddy simulation (LES)) are used to study the natural and actuated flows around an Ahmed body with no slanted surface at the rear, representing a squareback vehicle configuration. The results of these investigations are used to construct Reduced Order Models (ROM) with the purpose to increase our knowledge of these flows that can be used in construction of efficient control strategies. Previous work in the field considered 2-D geometries of the Ahmed body such as that in [1] and [2].
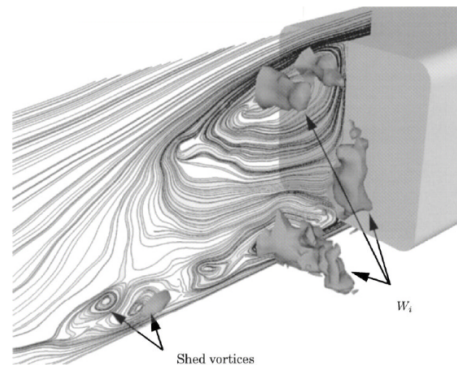

Figure 1. Instantaneous flow in the wake of an Ahmed body with no slanted surface from LES by [3]

The key flow mechanism of a 2-D geometry is a shear layer instability of the two shear layers emerging from the separated boundary layers at the rear end. As soon as they become unstable they interact forming a near wake bubble with typical low pressure at the rear base of the body. The 3-D geometry results in more complicated flow with additional two shear layers on the lateral sides and trailing vortices formed along the four longitudinal edges of the body. Such a flow was found in [3] to have more complex flow dynamics from the one found in the 2-D case characterized with periodic von Karman vortex shedding. For example the near-wake coherent structures shown in Fig. 1 originating from the four shear layers were found to be highly uncorrelated from each other.

This paper presents preliminary results from the on-

1

going collaborative research project by the authors. The set-up is a square-back vehicle bluff body. The flow around the body is studied both by wind tunnel experiments and by LES simulations and Reduced Order Modelling, at the moderate Reynolds number, $Re = 300\,000$, based on the height of the body.

2 Description of the set-up and the methods

This section presents the vehicle bluff body and numerical and experimental set-up.

2.1 The Ahmed body model

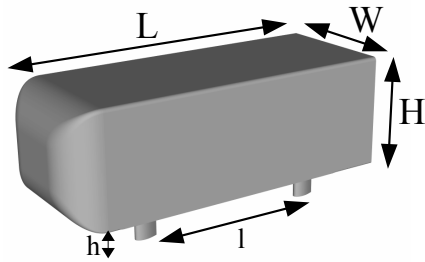The Ahmed reference model used in the present work is shown in Fig. 2.

Figure 2. Dimensions of the Ahmed model used in the present work.

The model has a square back geometry, but its dimensions are slightly different from the standard Ahmed body found in the literature. The length, L, is $0.893\,\mathrm{m}$, the width, W, is $0.35\,\mathrm{m}$ and the height of the body, H, is $0.297\,\mathrm{m}$. The front edges are rounded with a radius of $r = 0.285\,H$. The model is placed on four cylindrical supports with an oval-shaped cross section and the ground clearance h is $0.168\,H$ ($0.05\,\mathrm{m}$).

2.2 Experimental Setup

Measurements are performed in a closed-loop wind tunnel whose rectangular cross-section is $6.2\,\mathrm{m}^2$. The inlet velocity, U_0, in the wind tunnel is $15\,\mathrm{m/s}$. Turbulence intensity of the free-stream flow is around $0.3\,\%$. The model is mounted over an elliptical leading-edge flat plate in order to control the upstream boundary-layer thickness, such that it could be smaller than the ground clearance. The ensemble blockage ratio is $5.5\,\%$. Natural flow is studied by varying the Reynolds number and the ground clearance. Drag measurements, mean rear pressure, velocity data and flow visualizations were made. Open-loop actuation is done by periodic blowing generated from a continuous rectangular orifice tangential to the four trailing edges and with the direction of the upstream flow. The width, b, of the continuous slot is $0.0034\,H$ ($0.001\,\mathrm{m}$). An ensemble of 32 electrovalves provides a pulsed flow at a maximum velocity of $1.5U_0$ and a frequency range span from $0\,\mathrm{Hz}$ to $800\,\mathrm{Hz}$. For the velocities considered here, the large scale shedding frequency and the Kelvin-Helmholtz frequency are of order $10\,\mathrm{Hz}$ and $100\,\mathrm{Hz}$, respectively.
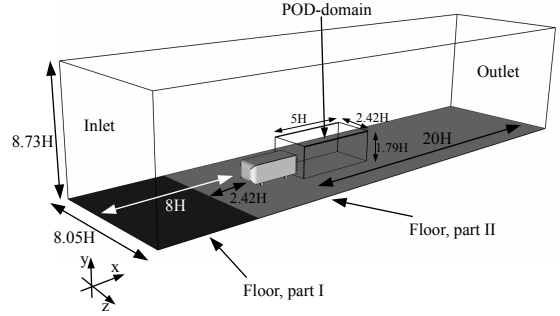
2.3 Numerical Setup

Figure 3. Computational domain used in the numerical simulations.

A numerical wind tunnel (see Fig. 3), with a cross-section corresponding to the part that is above the plate that is used to lift the Ahmed body in the the wind tunnel experiments, is constructed using the commercial grid generation software Ansys ICEM CFD. The computational grid is block-structured and contains only hexahedral elements. The number of grid points used in the simulation is 33 million. Time-resolved data are collected in a 3D domain in the wake (denoted POD-domain in Fig. 3). The data are used to decompose the flow field using the snaphot POD method [7]. The decomposition is then used as input for the Reduced Order Model.

2.4 Large Eddy Simulation

The governing filtered incompressible Navier-Stokes equations (Eqs. 1 and 2) are solved using a finite volume solver employing a collocated grid arrangement.

$$\frac{\partial \bar{u}_i}{\partial x_i} = 0. \tag{1}$$

$$\frac{\partial \bar{u}_i}{\partial t} + \frac{\partial}{\partial x_j}\left(\bar{u}_i \bar{u}_j\right) = -\frac{1}{\rho}\frac{\partial \bar{p}}{\partial x_i} + \nu \frac{\partial^2 \bar{u}_i}{\partial x_j \partial x_j} - \frac{\partial \tau_{ij}^r}{\partial x_j}. \tag{2}$$

The sub-grid stress is modeled by the dynamical Coherent-Structure Model (CSM) recently proposed in [4]. CSM is based on an eddy-viscosity representation of the sub-grid stress, $\tau_{ij}^r = -2\nu_{sgs}\bar{S}_{ij}$, where $\bar{S}_{ij}$ is rate-of-strain tensor of the filtered velocities and the length-scale Δ is taken to be the geometric average of the local grid size, $\Delta = (\Delta x \times \Delta y \times \Delta z)^{1/3}$. $\nu_{sgs} = C\Delta^2|\bar{S}|$ and the constant C is modeled by $C = C_1|F_{CS}|^{3/2}F_\Omega$ with $F_{CS} = Q/E$, $F_\Omega = 1 - F_{CS}$ and $C_1 = 1/22$. Q is the second invariant of the filtered velocity gradient tensor, $Q = -\frac{1}{2}\frac{\partial \bar{u}_i}{\partial x_j}\frac{\partial \bar{u}_j}{\partial x_i}$ and $E = \frac{1}{2}(\frac{\partial \bar{u}_j}{\partial x_i})^2$ is the magnitude of the filtered velocity gradient tensor. Thus, the Smagorinsky constant, C, is computed dynamically in each grid point and by the model it takes values ranging from $0 < C < 0.22$.

2

3 Results

This section presents preliminary results starting with global quantities and obtained resolution from the LES simulation, then continuing by presenting results from the actuated flow in the experiments.

3.1 Global quantities

Time-averaged aerodynamic forces from the LES simulation are presented in Table 1 and in Fig. 4 the time history of the drag signal is shown.
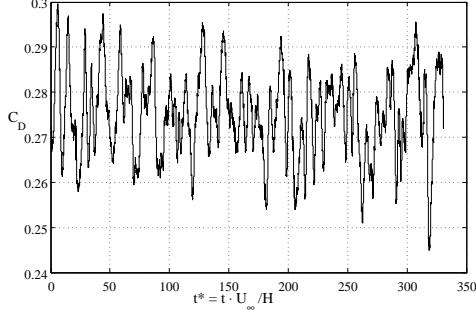

Figure 4. Time history of the drag signal from the LES simulation of the natural flow.

Table 1. Aerodynamic coefficients from LES.

	C_D	C_L	C_S
LES	0.275	-0.087	0.0064

3.2 Spatial resolution

The time-averaged spatial resolution on the body expressed in viscous wall units, $n^+ = \Delta n/\lambda^+$, $x^+ = \Delta x/\lambda^+$ and $s^+ = \Delta s/\lambda^+$, are presented in Table 2. Δn, Δx and Δs refer to the sizes of the cells in the wall-normal direction, streamwise direction and the spanwise directions, respectively. λ^+ is the viscous length scale defined as $\lambda^+ = \nu/u^*$ where u^* is the wall friction velocity. The size of the cells in normal direction on the body, n^+, is everywhere less than 1. The spatial- and time-average of the viscous length scale on the body, $< \lambda^+ >_t$, was computed to be $0.62 \cdot 10^{-5}$.

Table 2. Spatial resolution

	$< n^+ >_t$	$< x^+ >_{t,max}$	$< s^+ >_{t,max}$
LES	0.62	133	50

Figure 5 shows the streamwise velocity component in a plane cut in inner boundary layer on the roof. The figure reveals low and high speed streaks in the streamwise direction.
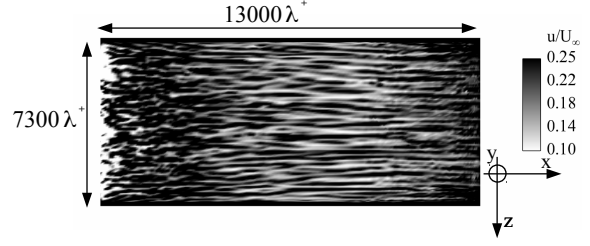

Figure 5. A plane cut from the LES simulation in the fifth cell layer away from the roof at approximately $y/\lambda^+ \approx 5$ showing regions of low and high streamwise velocities.

3.3 Experiments

Open-loop control along the four shear-layers separating from the sharp edges of the square back bluff body was performed. The pulsed plane jets are characterized by their frequency F_i and exit velocity, V_e, which varies from $\pm 10\%$ along the jet slit. The effects of control on the rear-pressure are analyzed. An increase of the back pressure, corresponding to a decrease of drag, is looked for. The exit velocity of the jets is directly related to the compressed-air pressure P_i, chosen in this work as a control parameter. A typical mean velocity profile at the exit of the jet as well as the dependence of V_e on P_i are illustrated in Fig. 6 for the case where $F_i = 0$ Hz (continuous blowing). The capability of pulsed
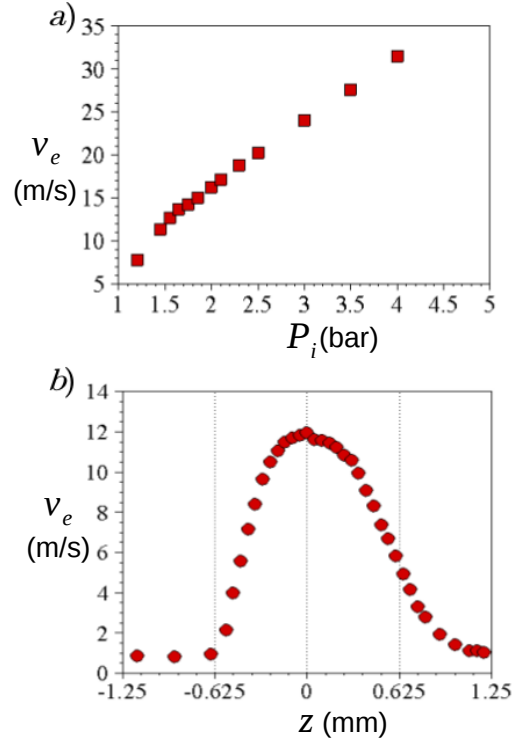

Figure 6. Control jet parameters ($F_i = 0$ Hz). a) dependence of V_e on P_i. b) velocity profile across the exit slit.

jets for changing rear pressure (and consequently drag) is investigated when $P_i = 1.45$ bar. Figure 7 shows the evolution of C_p/C_{p0} (rear pressure spatially averaged by the rear pressure spatially averaged for the natural flow) when the frequency F_i is varied.
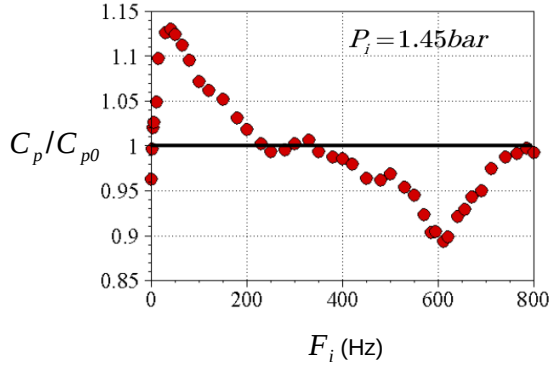
Figure 7. Influence of the control frequency F_i on the rear pressure (C_p/C_{p0}) (P_i= 1.45 bar)

We see clearly that pulsed jets can both increase or decrease the back pressure. Near frequencies of about 50 Hz, the back pressure decreases substantially. On the other hand, high-frequency forcing (610 Hz) increases considerably the rear pressure and then reduces drag. Taking this frequency constant ($F_i = 600$ Hz), the input pressure P_i is varied in order to verify the effect of the velocity amplitude of the pulsed jets. Figure 8 confirms the optimal gain in rear pressure increase when the exit velocity corresponds to the order of the upstream flow velocity. It is interesting to note that the gain drops sharply when the exit velocity is increased further.
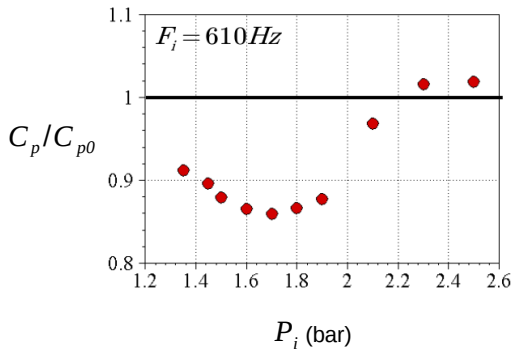

Figure 8. Influence of the control input pressure P_i on the rear pressure (C_p/C_{p0}) ($F_i = 610$ Hz)

Natural and controlled flows are now analyzed by means of velocity data taken from PIV on the symmetry plane of the Ahmed body. Figure 9 presents instantaneous vector velocity fields (colored by the norm of the velocity vector) for the uncontrolled configuration and for frequency forcing of 50 Hz (P_i =1.45 bar) and 610 Hz (P_i = 1.65 bar). Rolled-up structures on the upper shear layer as well as a recirculation region in the wake are identified on the natural flow. Low-frequency forcing seems to strengthen and anticipate the roll-up on the upper shear layer, generating a smaller recirculation region. Forcing at high frequencies changes slightly the direction of the shear layer development as well as promotes visually a flow stabilization effect, where roll-up of structures is less visible than the natural
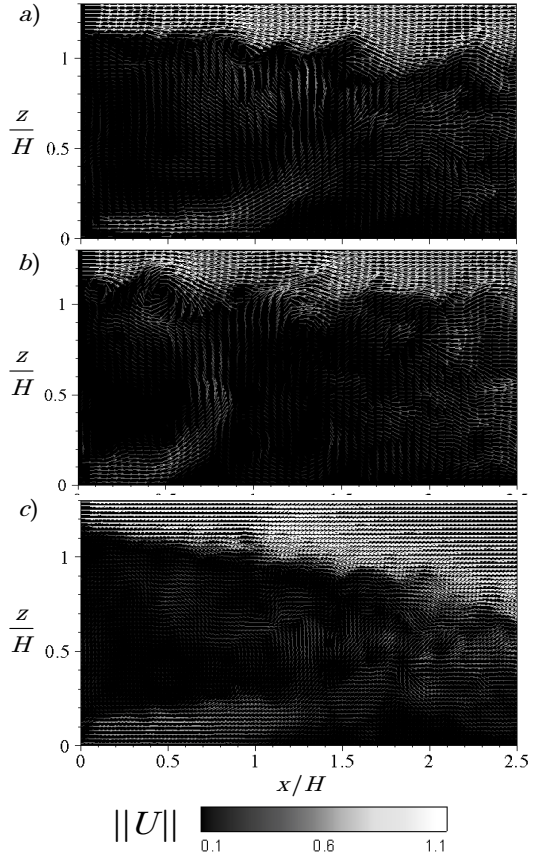
flow.

$$||U||$$

Figure 9. Instantaneous flow velocity vectors on the near wake. a) natural flow. b) low frequency forcing ($F_i = 50$ Hz and $P_i = 1.45$ bar). c) high-frequency forcing ($F_i = 610$ Hz and $P_i = 1.65$ bar). Vectors colored by their velocity magnitude.

Time-averaged fluctuating velocity is analyzed in order to detect shear layer and wake behavior. The Reynolds stresses are shown in Fig. 10 at the streamwise coordinate $x/H = 0.5$. First, we can observe that low-frequency forcing promotes a considerable increase in velocity fluctuations (both normal and shear stresses). Inversely, high-frequency actuation is capable of reducing these quantities as well as the direction of the upper-shear layer development, as observed for instantaneous flow (see Fig. 9 c).

3.4 Reduced-order model-based flow control

The reduced-order modelling shall lead to an empirical POD-based Galerkin model resolving the coherent structures of natural and actuated flow. The input data is 3D LES velocity fields. The first step leads to a Galerkin expansion

$$\boldsymbol{u}(\boldsymbol{x},t) = \boldsymbol{u}_0(\boldsymbol{x}) + \sum_{i=1}^{N} a_i(t)\, \boldsymbol{u}_i(\boldsymbol{x}) \qquad (3)$$
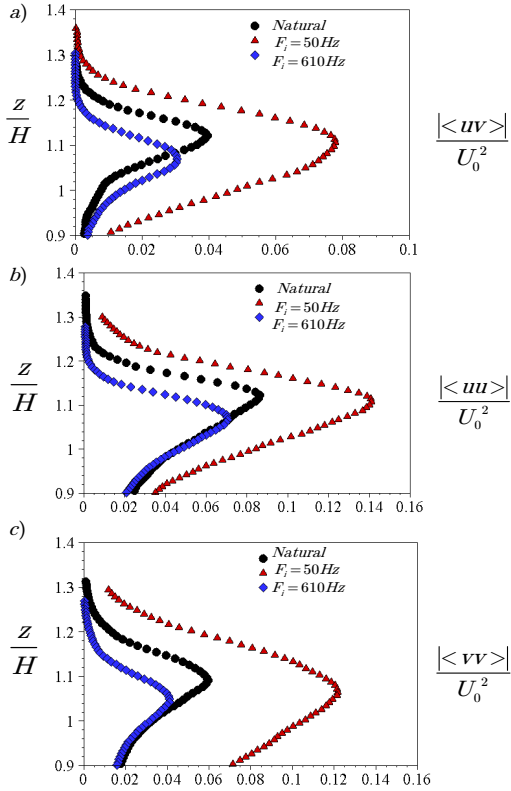
Figure 10. Reynolds stresses on the upper shear layer ($x/H = 0.5$). a) $\langle uv \rangle / U_0^2$ b) $\langle uu \rangle / U_0^2$. c) $\langle vv \rangle / U_0^2$.

with a base flow $\boldsymbol{u}_0$, N space dependent modes $\boldsymbol{u}_i$, $i = 1, \ldots, N$ and N corresponding mode amplitudes a_i, $i = 1, \ldots, N$. The second step is the identification of a dynamical system for unactuated and actuated conditions [5,6]:

$$\frac{d}{dt} a_i = c_i + \sum_{h=1}^{N} l_{ij} a_i + \sum_{j,k=1}^{N} q_{ijk} a_j a_k + g_i b, \qquad (4)$$

where c_i, l_{ij} and q_{ijk} are coefficients of the dynamical system, g_i the gains of the control and b the control amplitude. The purpose is to understand and improve the actuation employing the reduced-order model (ROM).

The ROM shall provide the crucial links between actuation (input), coherent structures (mode amplitudes) and pressure sensing (output) based on optimized open-loop experiments and the simulations. The resulting understanding of the physical actuation mechanisms, framed in control system dynamics, shall be employed for improved open- and closed-loop actuation, like in [2] and off-spring publications of the authors. The first mode from the Galerkin expansion (Eq. 3) is shown in Fig. 11. The figure shows an iso-surface of $Q = 50$, thus revealing areas where the vorticity is high in the flow. The iso-surface is colored by the vorticity around the streamwise axis.

4 Conclusions

The present paper has presented preliminary results from the ongoing research project involving Institute PPRIME at Université de Poitiers, Department of Applied
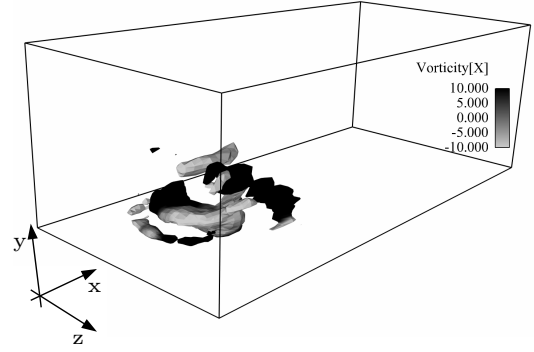

Figure 11. Visualization of the first mode of the POD decomposition.

Mechanics at Chalmers University of Technology and PSA Peugeot Citroën. The research in the project is dedicated to drag reduction of vehicles by active flow control. The project focuses on the fully 3D square back Ahmed body vehicle bluff body. Experimental, numerical and theoretical methods are used to meet the aims of the project. The experimental part consists of wind tunnel measurements of both natural and actuated flow around the body. The actuation is applied on all four edges on the base of the bluff body and consists of high frequency periodic blowing from a very small slit. The numerical part consists of time-resolved numerical simulations using the Large Eddy Simulation technique of the same set-up as the wind tunnel experiments. The theoretical method consists of using the high-resolved data from the simulation as input in a Galerkin system which is obtained by doing a flow decomposition using Proper Orthogonal Decomposition. From the modes obtained from the decomposition, a reduced number of modes, representative for the flow and for the physical mechanisms responsible for the induced aerodynamic drag on the body, are chosen for solving the reduced order dynamical system.

In the paper we have presented initial results from the simulation of the natural flow. A computational grid consisting of 34 million grid points was used in the LES simulation. The obtained spatial resolution was good enough for resolving the important flow processes.

As pointed out by [8], time-averaged fluctuating velocities can play an important role on the momentum balance of the wake region and consequently on the rear pressure. A possible explanation for such drag modifications can be the different mixing activity in the shear layers, confirmed in this work by the measured fluctuating velocities. Periodic forcing at high frequencies can be viewed as a promising strategy for drag reduction targeted control of three-dimensional bluff bodies. In the present case, these frequencies corresponds to a Strouhal number of $St = fH/U_0 = 12$ ($St_\theta = f \cdot \theta/(U_0/2) = 0.32$). This is significantly greater than the typical flow scales of the separated flow, namely the shear layer instabilities $St_\theta \approx 0.044$ [9] and the wake mode $St_H = 0.17$ [8].

Only the first mode from the POD decomposition was shown. The future work in the project consist of

performing additional LES simulations of actuated flow, building a reduced order model of both natural and actuation flow and gaining further insights from Reduced Order Modelling of the physical mechanisms causing drag.

5 Acknowledgements

REFERENCES

[1] Krajnović, S., and Fernandes, J., 2011 "Numerical Simulation of the Flow Around a Simplified Vehicle Model with Active Flow Control," *International Journal of Heat and Fluid Flow*, 32 (1), pp.192-200

[2] Pastoor M., Henning L., Noack B. R., King R. and Tadmor G. 2008 "Feedback shear layer control for bluff body drag reduction" *Journal of Fluid Mechanics*, 608, pp. 161-196

[3] Krajnović, S., and Davidson, L., 2003, "Numerical Study of the Flow Around the Bus-Shaped Body," *ASME: Journal of Fluids Engineering*, 125, pp. 500–509.

[4] Kobayashi, H., 2005, "The subgrid-scale models based on coherent structures for rotating homogeneous turbulence and turbulent channel flow," *The Physics of Fluids*, 17, 045104.

[5] Noack, B. R., Morzyński, M., & Tadmor, G. (editors) 2011 *Reduced-Order Modelling for Flow Control.* CISM Courses and Lectures n. **528**, Springer-Verlag Vienna.

[6] Cordier, L., Abou El Majd, B. & Favier, J. 2010 Calibration of POD reduced-order models by Tikhonov regularization.*Internat. J. Numer. Meth. Fluids.* **63** (2) 269–296.

[7] Sirovich, L. 1987 Turbulence and the dynamics of coherent structures, Parts I, II and III.*Quartely of Applied Mechanics XLV* 261–590.

[8] Grandemange, M., Gohlke, M., & Cadot, O., 2013 "Turbulent wake past a three-dimensional blunt body. Part 1. Global modes and bi-stability," *Journal of Fluid Mechanics*, 722, pp.51-84

[9] Ho, C. M. & Huerre, P., 1984 "Perturbed Free Shear Layers," *Annual Review of Fluid Mechanics*, 16, pp.365-422